Experimental Investigation of the Lithium Calendering Process for Direct Contact Prelithiation of Lithium-Ion Batteries

Benedikt Stumper,* Jonas Dhom, Lukas Schlosser, and Rüdiger Daub

Lithium-ion batteries suffer from high initial capacity losses during formation. One possible approach to compensate for these initial capacity losses is prelithiation, which is the addition of lithium into the battery cell before formation. A promising method is direct contact prelithiation using lithium foil, which requires lithium foil thicknesses below 10 μm to ensure the safe and accurate performance of the prelithiation process. However, free-standing lithium foils are only commercially available down to a thickness of 20 μm; hence, in this present work, the calendering process of lithium is investigated in detail. An already developed process model will be adapted to provide detailed information on the deformation properties and thickness reduction of different lithium foil thicknesses. A design of experiments is used to investigate the influences of lithium foil geometry, line load, web speed, and roller temperature on the deformation behavior of lithium during calendering. Lithium foil is applied onto anodes by calendering, which are electrochemically investigated using pouch cells. The cells prelithiated by calendering show improved electrochemical performance compared to the manually prelithiated cells, increasing cycle life by 19%.

1. Introduction

The transportation sector is currently transforming away from internal combustion engine vehicles to battery-powered electric vehicles (EVs) to reduce global greenhouse gas emissions. This shift is largely driven by efficient and cost-effective energy storage, and lithium-ion battery (LIB) technology is taking great prominence within it.[1,2] Despite their outstanding electrochemical properties, continuous improvement of LIBs in terms of energy density, cycle life, safety, and cost reduction is necessary to achieve the transition to electromobility.[3–5]

A significant increase in the capacity and energy density of LIBs is achieved using high-capacity electrode materials, such as silicon-based anodes. The specific capacity of silicon is about ten times higher than that of conventional graphite-based anodes ($3579\ \text{Ah}\,\text{kg}^{-1}$ vs. $372\ \text{Ah}\,\text{kg}^{-1}$).[6,7] However, the high capacity losses that occur due to the volume expansion of the silicon particles (by up to 300%) during charging and discharging processes make the commercial use of silicon-based anodes challenging.[8,9] These losses are mostly determined by the formation of the solid–electrolyte interphase (SEI), which consumes lithium ions.[10,11] The extent of the losses depends on the anode active material used and reduces the energy density and cycle life of LIB cells.[12]

So-called prelithiation has proven to be effective at compensating for these losses.[11,13–17] Prelithiation describes the introduction of additional lithium into the battery cell before formation. This compensates for the irreversible lithium losses that occur, increasing the initial capacity and, therefore, the energy density of the battery cell and the cycle life through the introduction of a lithium reservoir.[15] Prelithiation can be performed using different approaches, including chemical, electrochemical, and additive-based prelithiation, as well as direct contact prelithiation.[18]

Various prelithiation methods have already been investigated in the literature, but none of them has yet been implemented on an industrial scale. Direct contact prelithiation using lithium foil is considered a promising method due to its flexible application, compatibility with common electrode materials, scalability, and cost efficiency.[18,19]

For direct contact prelithiation with lithium foil, it is important that the amount of lithium is precisely adjusted and applied as areally and homogeneously as possible to the anode surface.[16,20] If too much lithium is applied to the anode, residues of metallic lithium can remain on the anode surface. These residues favor lithium plating and pose a safety risk due to possible dendrite growth.[21] For common anodes, only small amounts of lithium are required for prelithiation, and with today's commercially available lithium foils of down to 20 μm, it is not possible to apply lithium over the entire anode surface without exceeding the

B. Stumper, J. Dhom, L. Schlosser, R. Daub
TUM School of Engineering and Design
Department of Mechanical Engineering
Institute for Machine Tools and Industrial Management
Technical University of Munich
Boltzmannstraße 15, Garching 85748, Germany
E-mail: benedikt.stumper@tum.de

ADVANCED
SCIENCE NEWS

www.advancedsciencenews.com

Energy Technology
Generation, Conversion, Storage, Distribution

www.entechnol.de

required amount of lithium. It is, therefore, necessary to apply individual pieces of lithium, resulting in an inhomogeneous lithium distribution across the anode. To ensure uniform coverage of the anode surface with lithium foil without applying too much lithium, it is required to use a very thin lithium foil, typically less than 20 μm in thickness.[18] The specific thickness required varies depending on the type of anode material used. Additionally, achieving accurate prelithiation depends not only on using the thinnest possible lithium foil but also on selecting the appropriate foil thickness tailored to the specific anode material. Since the commercial availability of such thin and specific foils is challenging, it is important to understand the deformation behavior of lithium foil and investigate what minimum foil thicknesses can be achieved and how the thicknesses can be individually adjusted.

The calendering process, which is already an essential process within battery production to densify battery electrodes and improve their mechanical and electrochemical properties,[22,23] can be used to deform lithium foil and achieve the necessary lower thicknesses. For its realization and later utilization for direct contact prelithiation of LIB electrodes, a profound process comprehension and understanding of the deformation behavior of lithium during calendering is necessary.[24]

For this reason, the present work deals with the experimental investigation of the deformation of lithium foils by calendering and the model-based description of the deformation behavior. For this purpose, experimental data are generated using a systematic design of experiments. The experiments are conducted using a laboratory calender in an inert gas atmosphere (see Section 4). The corresponding experimental sample setup is also described in Section 4. For this purpose, lithium samples with defined geometries were calendered between two copper foils and the change in sample geometry after calendering was measured.

By supplementing experimental investigations with modeling the deformation behavior, a comprehensive and in-depth understanding of the processing and deformation of lithium foil can be achieved. A previously developed model is used,[24] which was optimized and extended within the scope of the present work.

2. Results and Discussion

2.1. Modeling of the Lithium Calendering Process

Within the present publication, the model developed by Stumper et al.[24] is used and adapted. The overall process model is a combination of empirical and analytical modeling. The model's input variables are different process variables and the geometry of the lithium foil (see **Figure 1**). The predicted thickness of the lithium foil after calendering obtained from the empirical model is further processed using analytical approaches. The model's output variables can fully describe the lithium geometry after deformation, which is of significant importance for the direct contact prelithiation process.[18]

Within the scope of the present publication, the original model is further modified. The model is defined for the subsequent three-dimensional factor space.

- $\vec{T}_R = [20, 40, 60, 80]$ °C
- $\vec{q}_L = [167, 500, 833, 1000, 1167]$ N mm^{-1}
- $h_0 = 50$ μm
- $v_w = 0.1$ m min^{-1}

Within the modified model, the regression equation was reduced by three coefficients (see Equation (1)), resulting in the same coefficient of determination, $R^2 = 0.99$. Therefore, fewer coefficients need to be determined, reducing the complexity of the model while the accuracy remains the same.

$$f(q_L, T_R) = k_1 + k_2 \cdot q_L + k_3 \cdot T_R + k_4 \cdot q_L^2 + k_5 \cdot q_L \cdot T_R + k_6 \cdot q_L^3 + k_7 \cdot q_L^2 \cdot T_R = \hat{h}_1 \tag{1}$$

To determine the coefficients k_{1-7}, the weighted least square method was applied using the experimentally obtained parameterization data.[25] Using the determined coefficients, Equation (1) provides the empirical model shown as a color-graded surface in **Figure 2**a in which the parameterization data are shown as blue points. The model allows the prediction of the
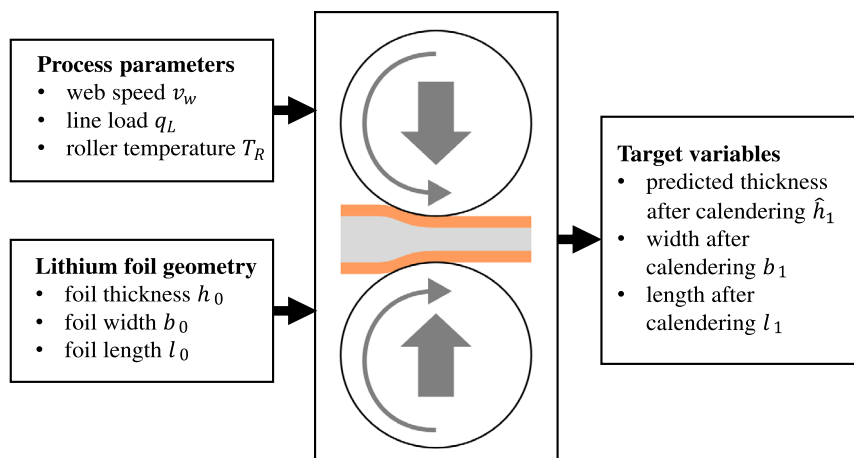

Figure 1. Schematic structure of the process model for the calendering of lithium foil with the considered process parameters and geometric variables of the lithium foil.[24]
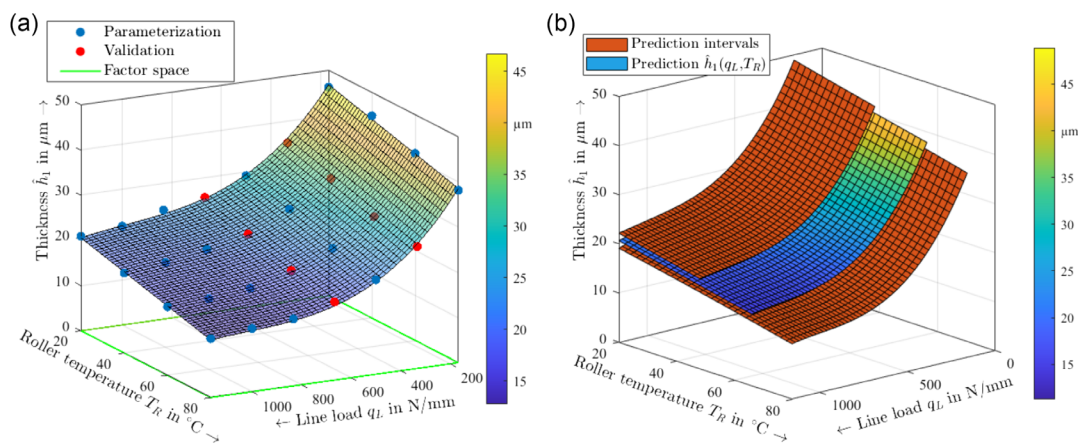
Figure 2. Representation of the empirical model for the defined factor space for $h_0 = 50\,\mu m$, $v_w = 0.1\,m\,min^{-1}$ with a) the respective parameterization data, validation data, and the factor space, and b) the illustration of the respective 95% prediction intervals for the model validation by the orange surfaces.

thickness of the lithium foil after calendering $\hat{h}_1$. The prediction is only valid in the factor space considered, which is outlined in green in Figure 2a. The validation of the model is performed using a prediction interval of 95%, and the experimentally obtained validation data are illustrated as red points in Figure 2a. The corresponding prediction intervals of 95% are illustrated in Figure 2b by the orange surfaces. For successful validation, the validation data must lie within these intervals.

In the context of the publication, the validation was successfully carried out for the initial foil thickness $h_0 = 50\,\mu m$, similar to Stumper et al.,[24] which leads to the confirmation that the modified model is also valid.

Subsequently, the scope of considered foil thicknesses is extended to additional foil thicknesses h_0 of 40, 30, and 20 μm within the scope of this publication. For this purpose, Equation (1) was used and reparameterized with new experimental data for the additional foil thicknesses. The corresponding empirical models are shown in **Figure 3**. It can be seen that the color-graded surfaces have shifted on the $\hat{h}_1$-axis, but all show a similar exponential progression. The validation described previously was also successfully performed for the additional foil thicknesses. This demonstrates that the empirical model can be used for any foil thickness after the respective parameterization and validation.

2.2. Experimental Investigation of Lithium Calendering

For direct contact prelithiation of currently used anode materials, the lithium foil thickness needs to be very low and precisely adjusted to be able to apply a lithium foil to the anode with as large an area as possible. A calendering process can be used to achieve these low and precise lithium foil thicknesses.[18] Therefore, it is important to get an in-depth understanding of the calendering and deformation behavior of lithium foils. When lithium foil is calendered, not only the thickness but also the area of the foil changes.[24] However, the focus of this publication is on acquiring knowledge about reducing the thickness of lithium foil and the minimum foil thicknesses that can be
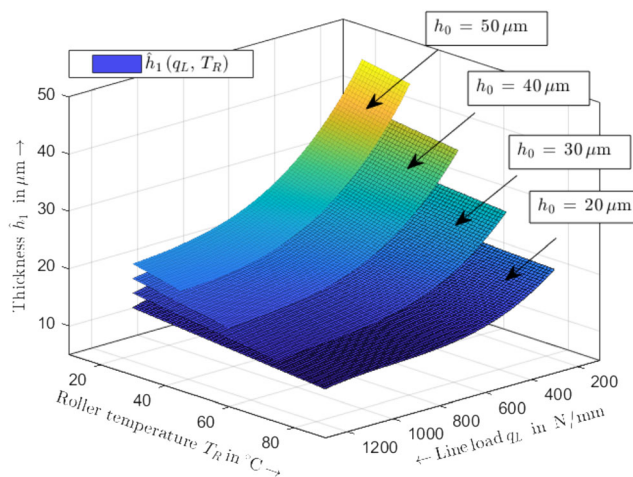

Figure 3. Schematic representation of the empirical models for different lithium foils input thicknesses h_0 of 50, 40, 30, and 20 μm, for the web speed $v_w = 0.1\,m\,min^{-1}$. The model was created and plotted for each considered foil thickness. For visualization, the surfaces are shown in gradual stages.

achieved. Therefore, the area changes are not considered in the following investigations, although these must not be disregarded when actually applying lithium foil pieces to the anode in a prelithiation context. For the lithium calendering investigations, different foil thicknesses are calendered at different line loads and roller temperatures. **Figure 4** shows the experimental results for different lithium foil thicknesses h_0 of (a) 50 μm, (b) 40 μm, (c) 30 μm, and (d) 20 μm at different roller temperatures T_R (20, 40, 60, and 80 °C) and at a constant web speed of $v_w = 0.1\,m\,min^{-1}$.

The experimental results show that at higher roller temperatures, the deformation behavior of the lithium foil changes. This is due to the significant reduction in the mechanical properties of lithium at elevated temperatures.[26] This deformation behavior is also described for the calendering of cathodes, where the
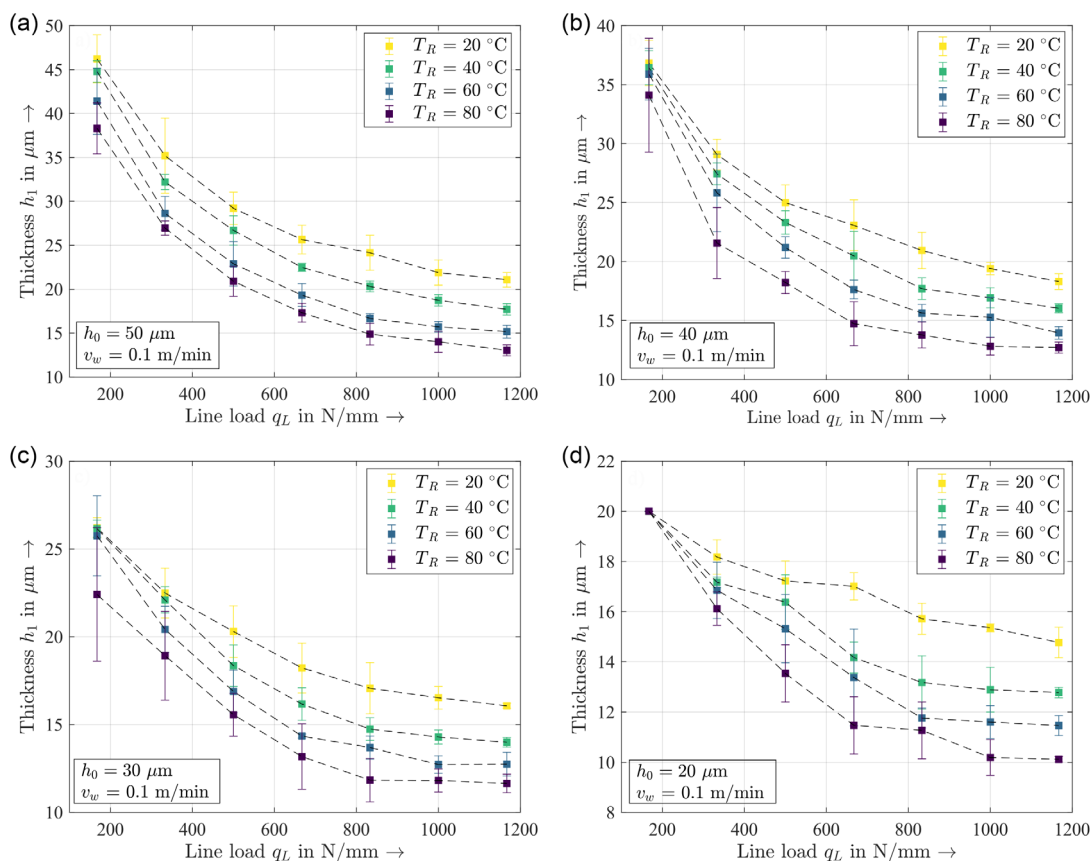
Figure 4. Influence of the roller temperatures T_R for h_0 values of a) 50 μm, b) 40 μm, c) 30 μm, and d) 20 μm at a web speed $v_w = 0.1$ m min^{-1}. The mean values and standard deviations refer to five measured values in each case. Note: For the foil thickness of 20 μm, there was no deformation at the lowest line load investigated. Since the foil thickness is subject to tolerance-related deviations, the nominal value of the 20 μm foil was set as the starting value.

porosity reduction, and therefore the thickness reduction, is increased at higher roller temperatures. The line load is another process parameter that strongly influences the thickness reduction, which is also similar to the calendering of cathodes.[27]

For each lithium foil used, it can be seen that for the considered line loads, further deformation decreases with increasing line loads. Comparing, for example, the deformation behavior of the lithium foils with a thickness of 50 and 20 μm, it can be seen that a thicker foil can be deformed relatively more than a thinner one. This leads to the conclusion that lithium becomes harder to deform the thinner it gets, which makes the production of ultrathin lithium foils difficult and hinders their commercial availability.

The plastic deformation of lithium is further analyzed to obtain a deeper understanding of its calendering behavior. In plastic deformation, two limits restrict the deformation behavior of materials. The deformation capacity is a material-specific parameter that restricts the deformation process, whereas the forming limit is a process-specific variable.[28] The deformation capacity within calendering depends on the calendered material, roller temperature, web speed, and type of stress state in the material.[28] The condition of the material results from the chemical composition (e.g., alloy elements), the material structure

(e.g., grain size), the heat treatment (e.g., soft annealing, recrystallization annealing, tempering, quenching, and tempering), as well as the processing step during the production (e.g., casting, forging, rolling). The deformation capacity of the material increases at a higher roller temperature, as shown in Figure 4. The web speed also has a significant influence on the deformation capacity of the material. The deformation increases the longer the force is applied to the lithium foil. Thus, the deformation capacity decreases with higher web speed and is also strongly dependent on the stress state of the material. This state of stress can be divided into a deviatoric and a hydrostatic part. The deviator stresses are mainly responsible for the plastic flow, while the hydrostatic part is decisive for the deformation capacity of the material.[28]

In Figure 4, all of the lithium foils with different h_0 are provided by the same manufacturer; therefore, it can be assumed that the chemical composition of the lithium is the same. T_R and v_w were also identical for the values examined. Since the hydrostatic stress depends, among others, on the geometry of the lithium foil, the lithium foil deforms differently at different h_0. The width and length of the lithium are always the same in Figure 4, and h_0 is the only varying geometric parameter. Therefore, h_0 influences the deformation capacity.

**ADVANCED
SCIENCE NEWS**
www.advancedsciencenews.com

Energy Technology
Generation, Conversion, Storage, Distribution
www.entechnol.de

Consequently, the lithium foil can be deformed to a greater extent if h_0 is increased.

In order to get an overview of the maximum thickness reduction that has been achieved during the calendering of lithium, **Table 1** shows the maximum thickness reduction for h_0 of 50, 40, 30, and 20 μm at $q_L = 1167$ N mm^{-1}, $T_R = 80$ °C, and, $v_w = 0.1$ m min^{-1}. It can be seen that the lowest thickness of $h_1 = 10.12 \pm 0.11$ μm was obtained with the input foil thickness $h_0 = 20$ μm. Table 1 shows that larger input thicknesses are deformed significantly more than thinner input thicknesses, which was described previously.

Another important process parameter influencing the thickness reduction during calendering is the web speed v_w.[29] Therefore, further calendering studies were conducted at elevated web speeds. These were carried out for the thickest (50 μm) and the thinnest (20 μm) lithium foils considered at $T_R = 20$ °C, which are shown in **Figure 5**a,b, respectively. The influence of the web speed on the thickness reduction is investigated using the three different calendering web speeds v_w (0.1, 0.5, and 1.0 m min^{-1}).

As with the calendering of battery electrodes, the thickness reduction decreases with increasing web speed.[29] This can be explained by the reduced contact time of the lithium foil within the calender gap and, thus, reduced deformation duration for the material. Yet again, despite the increasing line load, the deformation is highest in percentage terms at the beginning of the

Figure 6. Schematic representation for the evaluation of the lithium geometry 18 mm × 55 mm by the prediction intervals for $h_0 = 50$ μm, $v_w = 0.1$ m min^{-1}, $T_R = 20$ °C. The mean values and standard deviations refer to three measured values in each case.

considered line loads. This behavior is evident from the slope of the deformation, which is highest at the beginning.

In order to verify if the deformation behavior of the lithium foil is geometry independent, additional investigations are performed for a larger foil geometry of 18 mm × 55 mm. The model described in Section 2.1 is used to investigate the assumption, which is parameterized and validated with the lithium geometry 18 mm × 18 mm. For this purpose, the model is transferred into the 2D factor space with the respective prediction intervals of 95% (see **Figure 6**).

Five different line loads are used for the investigation. The respective experimental data are shown in Figure 6, and it can be seen that they are all within the 95% prediction intervals. It is, therefore, assumed that the thickness reduction during calendering of the lithium foil is independent of the lithium foil geometry.

Table 1. Comparison of the maximum thickness reduction Δh for h_0 of 50, 40, 30, and 20 μm at $q_L = 1167$ N mm^{-1}, $T_R = 80$ °C, and $v_w = 0.1$ m min^{-1}. The mean values and standard deviations refer to five measured values in each case.

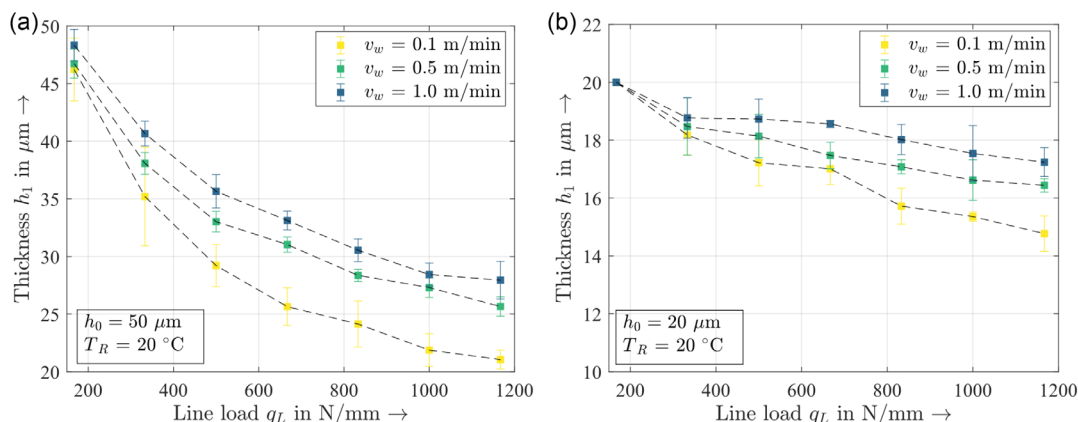| Input thickness h_0 [μm]	Output thickness h_1 [μm]	Thickness reduction Δh [μm]	Relative thickness reduction [%]
20	10.12 ± 0.11	9.88	49.40
30	11.65 ± 0.53	18.35	61.20
40	12.70 ± 0.47	27.30	68.25
50	13.03 ± 0.62	36.97	73.94

Figure 5. Influence of different web speeds v_w (0.1, 0.5, and 1.0 m min^{-1}) on the deformation behavior of lithium foil at $T_R = 20$ °C for a) $h_0 = 50$ μm and b) $h_0 = 20$ μm. The mean values and standard deviations refer to five measured values in each case. Note: For the foil thickness of 20 μm, there was no deformation at the lowest line load investigated. Since the foil thickness is subject to tolerance-related deviations, the nominal value of the 20 μm foil was set as the starting value.
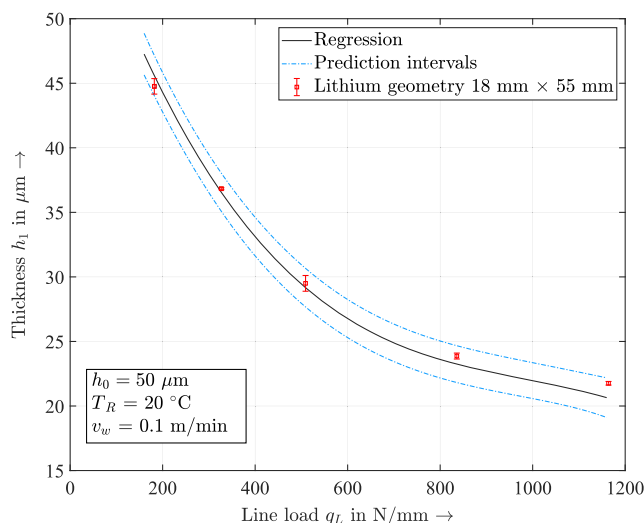
2.3. Application of Lithium Foil via Calendering for Direct Contact Prelithiation

Within the previous section, the thickness reduction of lithium foil by calendering was described. In the following sections, the utilization of the calendering process for the application of lithium foil onto anodes for direct contact prelithiation is evaluated, and the respective proof of concept is carried out. In this context, process parameters are selected to ensure that neither the lithium foil nor the anode is deformed, which are different from the process parameters for the lithium foil thickness reduction. The process of applying lithium foil to the anode surface is therefore considered separately from the previously shown lithium foil deformation experiments. The sample setup is changed from lithium rolled between two copper foils to the setup described in the second part of the experimental section consisting of copper foil, anode coating, lithium foil, Mylar foil, and copper foil.

Due to the surface roughness of the anode surface, there are only a few direct contact areas between the anode and the lithium foil when applying the lithium manually with little or no pressure, highlighted in yellow in **Figure 7**a. Few contact areas between the lithium foil and the anode surface lead to poor electron transfer and, thus, to slower and inhomogeneous prelithiation.[11] In order to increase the contact area, the lithium foil is pressed into the inhomogeneities and pores on the anode surface by calendering without deforming the lithium foil or the anode (see Figure 7b). This results in a larger contact area and better contact between the lithium and the anode, which is advantageous for direct contact prelithiation. A similar approach has already been used by Meng et al.,[11] where a conductive layer was used to establish electrical contact between the lithium and the anode, thus compensating for the anode surface irregularities by bridging the gaps between both surfaces. The conductive layer facilitates the transport of electrons from the lithium foil into the anode, which is no longer necessary when the lithium is pressed directly into the inhomogeneities and pores of the anode surface.

To investigate this effect, lithium foil is calendered onto silicon–graphite anodes, which are assembled in single-layer pouch cells versus NMC622 cathodes and electrochemically

tested. **Figure 8**a shows the open-circuit voltage (OCV) measurements during the prelithiation of these pouch cells. The figure shows the voltage curves of two different pouch cell configurations, one in which lithium was applied to the anode manually (yellow) and the other in which lithium was calendered onto the anode (green). The same cell setup and the same amount of lithium were used for both configurations. The applied lithium foil pieces were circular with a diameter of 20 mm, which corresponds to about 28% of the total anode capacity (calculated nominal anode capacity of 45.49 mAh).

The increase in voltage indicates a progressive prelithiation of the anode due to the continuous deposition of lithium in the anode active material.[30] A detailed explanation and discussion of the OCV measurements for the same anode material have already been performed in a previous publication.[30]

The green curve of the pouch cells prelithiated by calendering achieves a flatter course and a lower maximum voltage. This indicates that the prelithiation is slower than for the manually prelithiated anodes, which can be attributed to the better contact between the lithium and the anode for the calendered anodes. The pores of the anode surface are filled with lithium due to the better contact, which prevents the anode from being completely wetted. However, with increasing electrolyte wetting, prelithiation can be accelerated. The larger deviations, illustrated by the error bars of the standard deviations in Figure 8a, could also be caused by an impeded wetting of the anode. The improved contact between the lithium foil and the anode impairs the wetting at the direct contact areas, which causes the lithium deposition into the anode to proceed at different velocities. However, since the error bars decrease with increasing observation time, this suggests that after complete wetting of the anode, prelithiation also homogenizes within the considered cells. It can be observed that the curve of the manually prelithiated anodes flattens out earlier, whereas the course of the calendered anodes continues to rise until the end of the observation period. It can be deduced that the two curves converge to a similar level if the observation period is long enough, which leads to the assumption that, although spontaneous, self-sustained prelithiation is slowed down by calendering, the degree of prelithiation is not reduced. Even if the voltage maxima are not the same for both configurations, a lower voltage level reached
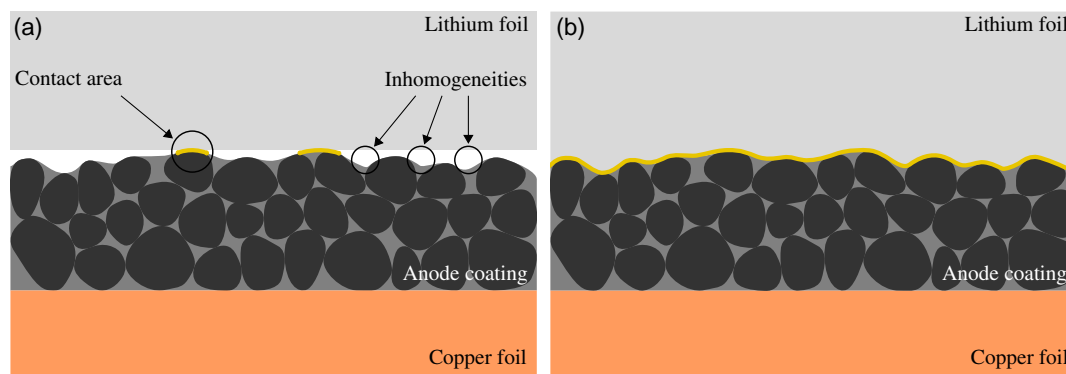

Figure 7. Illustration of the effect of calendering lithium onto the anode surface. a) Lithium is applied without pressure with only a few contact areas to the anode. b) Increase in the contact area between the lithium foil and the anode by calendering the lithium into the inhomogeneities of the anode surface. The contact area between lithium and the anode is highlighted in yellow.
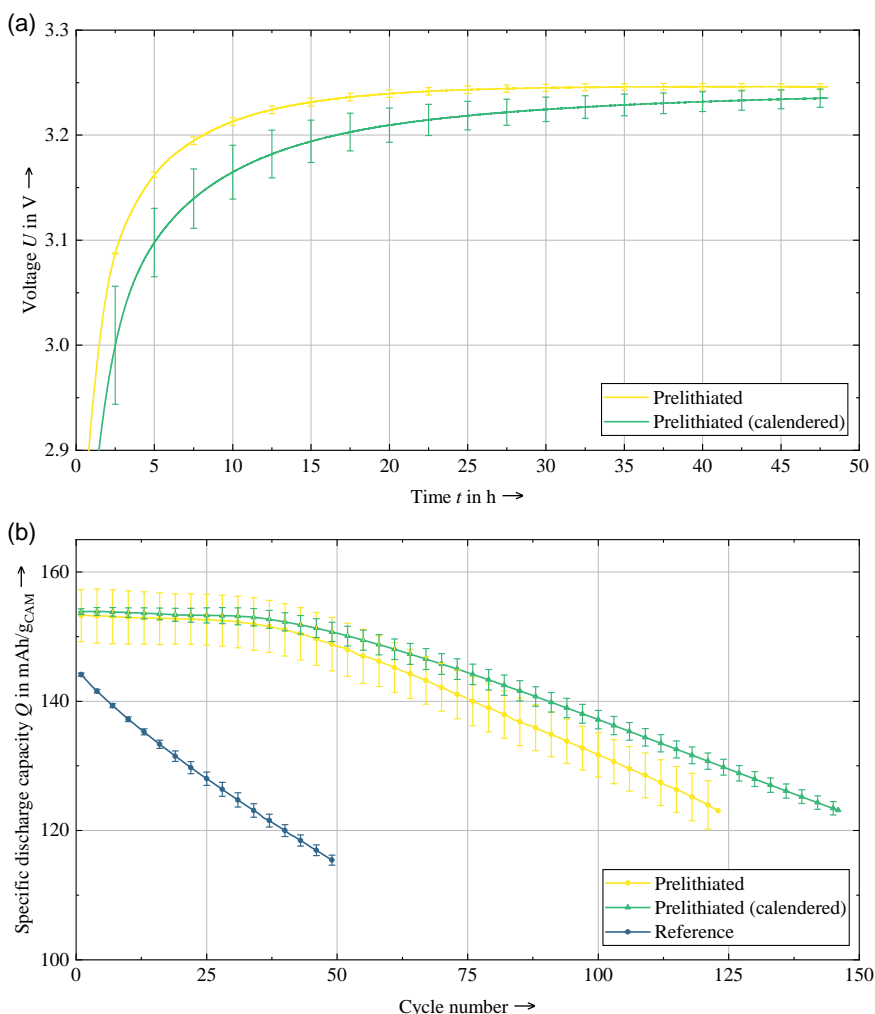
Figure 8. Influence of the calender-based lithium foil application for direct contact prelithiation and its impact on the performance of NMC622 versus silicon–graphite single-layer pouch cells. a) OCV measurements during 48 h prelithiation time and b) cycle life investigations.

may also indicate an earlier set equilibrium between lithium incorporation into the anode and its distribution within the anode.[30,31]

Figure 8b shows the specific discharge capacities of the respective prelithiated pouch cells. Both prelithiation configurations show a significantly higher initial capacity and improved cycle life compared to the unprelithiated reference cells. In addition, lithium calendering shows a further improvement. It is shown that the difference in OCV measurements is not reflected in the discharge capacities. The cells with lithium applied onto the anodes by calendering show slightly increased initial capacities of 153.86 ± 0.46 mAh g_{CAM}^{-1} compared to the cells with manually applied lithium of 153.26 ± 4.04 mAh g_{CAM}^{-1}, although the voltages during the OCV measurement were lower for the cells prelithiated by calendering than for the manually prelithiated cells. The standard deviation is also significantly reduced by calendering, indicating that prelithiation reproducibility is improved by calendering. Additionally, the cells that have been prelithiated by calendering show improved capacity retention, which is reflected in the flatter curve progression. The manually

prelithiated cells reach 80% of their initial capacity (end of life) at 124 cycles, whereas the cells prelithiated by calendering reach 80% capacity retention at 147 cycles, which is an increase in cycle life of almost 19%. The improvement in prelithiation can be explained by the hypothesis that the calendering of the lithium foil onto the anode surface creates better contact between the lithium and the anode, which promotes prelithiation and the formation of an improved lithium reservoir. These findings indicate that the prelithiation of the anode can be improved by applying the lithium by calendering, which in turn suggests that this method provides a further improvement in the direct contact prelithiation process.

3. Conclusion

The application and processing of metallic lithium are becoming increasingly relevant in the context of LIBs and post-LIBs.[32] Especially processing steps within the process chain of battery production, such as the cutting and separating[33] or handling of lithium,[34,35] are the focus of scientific investigations. For this reason, this work focuses on the calendering of lithium and its

deposition onto battery electrodes in the context of direct contact prelithiation of LIB. Very thin lithium foils or precisely adjusted foil pieces with defined geometric dimensions are required to enable direct contact prelithiation using lithium foil for LIB production. Therefore, an in-depth understanding of the calendering and deformation process of lithium foil is essential to ensure a precise prelithiation process, as well as safe and efficient cell operation. The deformation behavior of lithium foil was analyzed through extensive experimental investigations and model-based approaches.

The presented model provides an in-depth understanding of the deformation process, which can reduce the experimental effort. The transfer of the model to different calenders is possible if new experiments are conducted to parameterize and validate the model for the respective calender.

The experimental investigation of the calendering behavior of lithium showed that high roller temperatures and line loads lead to higher deformation of lithium, while high web speeds lead to lower deformation. In addition, it was shown that the decrease in thickness during calendering is independent of the lithium geometry.

The performed electrochemical cell tests showed that direct contact prelithiation could be successfully performed by calender-based lithium application onto the anode. This approach could compensate for a large part of the lithium loss and can potentially be adapted as a roll-to-roll approach within battery production, which leads to an economic advantage compared to other prelithiation methods. Furthermore, the findings of the present work can be applied to the field of lithium metal anodes for all-solid-state batteries.

4. Experimental Section

First Part of Experimental Section: The experiments within the scope of this work were carried out using a laboratory calender (GK 300 L, SAUERESSIG Group, Germany) enclosed in a glovebox system (GS GLOVEBOX Systemtechnik GmbH, Germany) in an argon atmosphere ($O_2 < 0.5$ ppm, $H_2O < 0.5$ ppm, temperature $\sim 20\,°C$). The calender setup within the glovebox is shown on the left of **Figure 9**. As carrier foils for the sample setup, copper foils (SE-Cu/Cu-HCP, Schlenk Metallfolien
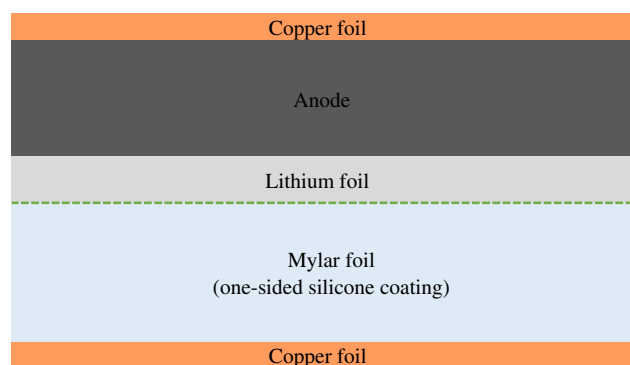

Figure 10. Schematic illustration of the sample setup for the conducted experiments for the calender-based application of lithium foil for direct contact prelithiation (Section 2.3).

GmbH & Co. KG, Germany) with thicknesses of 12 μm were used for all experiments. The lithium foils had thicknesses of 20, 30, 40, and 50 μm and a purity of 99.9% (China Energy Lithium Co. LTD, China). If not explicitly mentioned otherwise, the lithium samples used for the experiments each had a length and width of 18 mm ($b_0 = l_0$), respectively. For the conducted experiments, the sample setup, which is shown on the right of Figure 9, was prepared accordingly and then fed into the calender. The thickness of the lithium foil was measured after calendering using a tactile measuring device (MarCator 1086 R-HR, Mahr GmbH, Germany) with a resolution of 0.1 μm. The samples were measured on a static measuring table, which allowed the exact determination of the thickness within the glovebox.

Second Part of Experimental Section: For the investigations on the transferability of the lithium calendering to direct contact prelithiation, the setup already described in the previous section was used. However, the sample setup was modified, as shown in **Figure 10**. Instead of one of the copper foils, a silicon–graphite anode was used onto which the lithium was calendered with a line load of 60.61 N mm^{-1}, $T_R = 20\,°C$, and $v_w = 0.1$ m min^{-1}. A Mylar foil (PPI 0601, PPI Adhesive Products GmbH, Germany) was inserted between the lithium and copper foil to prevent lithium from adhering to the copper foil on the other side. The Mylar foil had a silicone coating (green dashed line) on the lithium side so that it could be removed again after calendering without detaching the lithium from the anode.

The same electrode materials and cell components were used for both the unprelithiated reference cells and the prelithiated cells.
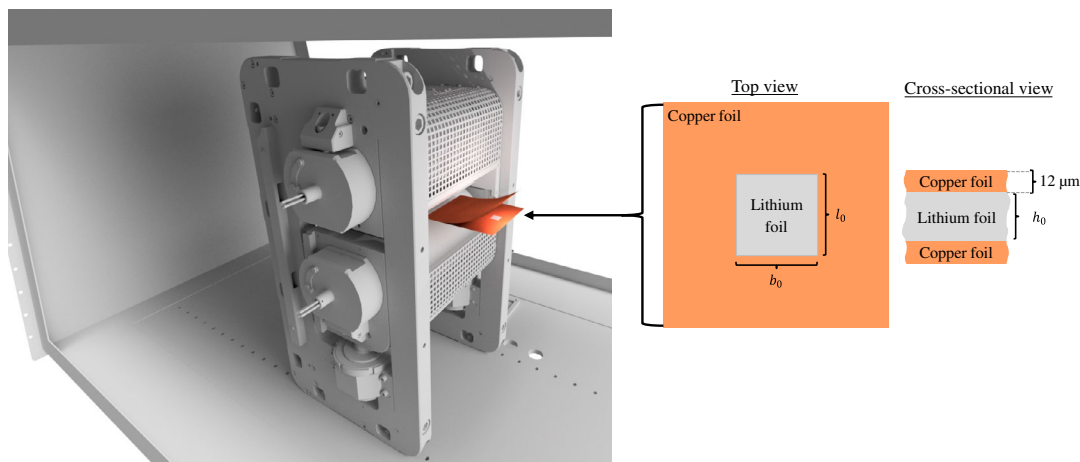

Figure 9. Schematic illustration of the sample setup for the conducted experiments. The laboratory calender integrated into a glovebox is shown on the left, and the multilayered copper and lithium foil sample setup is on the right.

The silicon–graphite anodes used consisted of 94 wt% active material, 1 wt% conductive carbon black (C-65), 2 wt% carboxymethyl cellulose (CMC), and 3 wt% styrene-butadiene rubber (SBR). The active material was composed of ≈90 wt% graphite and 10 wt% carbon-coated crystalline silicon. The anode dimensions were ≈33 mm × 33 mm, and the areal capacity was 4.2 mAh cm^{-2}. The cathodes used were LiNi$_{0.6}$Mn$_{0.2}$Co$_{0.2}$O$_2$ (NMC622) cathodes consisting of 95.5 wt% NMC622 cathode active material (CAM), 1.5 wt% conductive carbon black (C-65), 0.75 wt% SFG6L, and 2.25 wt% PVDF binder with dimensions of ≈30 mm × 30 mm and an areal capacity of 3.8 mAh cm^{-2}. A glass fiber separator with 90% porosity (VWR International GmbH, Germany) was used for the cell setup. The electrolyte used for the pouch cells was a 1M solution of lithium hexafluorophosphate (LiPF$_6$) in a mixture of ethyl carbonate (EC) and ethyl methyl carbonate (EMC) in a weight ratio of EC:EMC of 3:7 with 2 wt% vinyl carbonate (LP572, BASF SE, Germany). The electrochemical cell tests were conducted using a battery cell test system (CTS, BaSyTec GmbH, Germany). The formation of the cells was conducted at C/10 for 3 cycles between 3.0 and 4.2 V, followed by cycle life testing at C/3 in the same voltage range at ≈25 °C. Three cells each were built and tested for the described investigations. The reference cells were built without additional lithium foil, and for the prelithiated cells, the lithium foil was either applied manually or via calendering.

Acknowledgements

Conflict of Interest

The authors declare no conflict of interest.

Data Availability Statement

The data that support the findings of this study are available from the corresponding author upon reasonable request.

Keywords

[1] D. Bresser, K. Hosoi, D. Howell, H. Li, H. Zeisel, K. Amine, S. Passerini, *J. Power Sources* **2018**, *382*, 176.

[2] M. Armand, P. Axmann, D. Bresser, M. Copley, K. Edström, C. Ekberg, D. Guyomard, B. Lestriez, P. Novák, M. Petranikova, W. Porcher, S. Trabesinger, M. Wohlfahrt-Mehrens, H. Zhang, *J. Power Sources* **2020**, *479*, 228708.

[3] A. Kwade, W. Haselrieder, R. Leithoff, A. Modlinger, F. Dietrich, K. Droeder, *Nat. Energy* **2018**, *3*, 290.

[4] P. Lamp, in *Lithium-Ion Batteries: Basics and Applications*, (Eds: R. Korthauer), Springer Berlin Heidelberg, Berlin **2018**, pp. 371–391, ISBN 978-3-662-53069-6.

[5] N. Nitta, F. Wu, J. T. Lee, G. Yushin, *Mater. Today* **2015**, *18*, 252.

[6] B. Scrosati, J. Garche, *J. Power Sources* **2010**, *195*, 2419.

[7] H. Tian, F. Xin, X. Wang, W. He, W. Han, *J. Materiomics* **2015**, *1*, 153.

[8] J. W. Choi, D. Aurbach, *Nat. Rev. Mater.* **2016**, *1*, 4.

[9] M. T. McDowell, S. W. Lee, W. D. Nix, Y. Cui, *Adv. Mater.* **2013**, *25*, 4966.

[10] M. Ashuri, Q. He, L. L. Shaw, *Nanoscale* **2016**, *8*, 74.

[11] Q. Meng, G. Li, J. Yue, Q. Xu, Y.-X. Yin, Y.-G. Guo, *ACS Appl. Mater. Interfaces* **2019**, *11*, 32062.

[12] J. B. Goodenough, K.-S. Park, *J. Am. Chem. Soc.* **2013**, *135*, 1167.

[13] P. Bärmann, M. Diehl, L. Göbel, M. Ruttert, S. Nowak, M. Winter, T. Placke, *J. Power Sources* **2020**, *464*, 228224.

[14] C. L. Berhaut, D. Z. Dominguez, D. Tomasi, C. Vincens, C. Haon, Y. Reynier, W. Porcher, N. Boudet, N. Blanc, G. A. Chahine, S. Tardif, S. Pouget, S. Lyonnard, *Energy Storage Mater.* **2020**, *29*, 190.

[15] V. L. Chevrier, L. Liu, R. Wohl, A. Chandrasoma, J. A. Vega, K. W. Eberman, P. Stegmaier, E. Figgemeier, *J. Electrochem. Soc.* **2018**, *165*, A1129.

[16] A. Shellikeri, V. Watson, D. Adams, E. E. Kalu, J. A. Read, T. R. Jow, J. S. Zheng, J. P. Zheng, *J. Electrochem. Soc.* **2017**, *164*, A3914.

[17] Z. Wang, Y. Fu, Z. Zhang, S. Yuan, K. Amine, V. Battaglia, G. Liu, *J. Power Sources* **2014**, *260*, 57.

[18] B. Stumper, A. Mayr, G. Reinhart, *Procedia CIRP* **2020**, *93*, 156.

[19] F. Holtstiege, P. Bärmann, R. Nölle, M. Winter, T. Placke, *Batteries* **2018**, *4*, 4.

[20] F. Holtstiege, R. Schmuch, M. Winter, G. Brunklaus, T. Placke, *J. Power Sources* **2018**, *378*, 522.

[21] V. Zinth, C. von Lüders, M. Hofmann, J. Hattendorff, I. Buchberger, S. Erhard, J. Rebelo-Kornmeier, A. Jossen, R. Gilles, *J. Power Sources* **2014**, *271*, 152.

[22] N. Billot, T. Günther, D. Schreiner, R. Stahl, J. Kranner, M. Beyer, G. Reinhart, *Energy Technol.* **2020**, *8*, 1801136.

[23] D. Schreiner, T. Zünd, F. J. Günter, L. Kraft, B. Stumper, F. Linsenmann, M. Schüßler, R. Wilhelm, A. Jossen, G. Reinhart, H. A. Gasteiger, *J. Electrochem. Soc.* **2021**, *168*, 030507.

[24] B. Stumper, J. Dhom, L. Schlosser, D. Schreiner, A. Mayr, R. Daub, *Procedia CIRP* **2022**, *107*, 984.

[25] L. Fahrmeir, T. Kneib, S. Lang, B. D. Marx, *Regression: Models, Methods and Applications*, Springer Berlin Heidelberg, Berlin **2021**.

[26] W. S. LePage, Y. Chen, E. Kazyak, K.-H. Chen, A. J. Sanchez, A. Poli, E. M. Arruda, M. D. Thouless, N. P. Dasgupta, *J. Electrochem. Soc.* **2019**, *166*, A89.

[27] C. Meyer, M. Weyhe, W. Haselrieder, A. Kwade, *Energy Technol.* **2020**, *8*, 1900175.

[28] F. Klocke, *Fertigungsverfahren 4: Umformen, VDI-Buch*, Springer Vieweg, Berlin **2017**.

[29] C. Meyer, H. Bockholt, W. Haselrieder, A. Kwade, *J. Mater. Process. Technol.* **2017**, *249*, 172.

[30] B. Stumper, A. Mayr, K. Mosler, J. Kriegler, R. Daub, *J. Electrochem. Soc.* **2023**, *170*, 060518.

[31] C. Hogrefe, S. Hein, T. Waldmann, T. Danner, K. Richter, A. Latz, M. Wohlfahrt-Mehrens, *J. Electrochem. Soc.* **2020**, *167*, 140546.

[32] J. Schnell, T. Günther, T. Knoche, C. Vieider, L. Köhler, A. Just, M. Keller, S. Passerini, G. Reinhart, *J. Power Sources* **2018**, *382*, 160.

[33] J. Kriegler, T. M. Duy Nguyen, L. Tomcic, L. Hille, S. Grabmann, E. I. Jaimez-Farnham, M. F. Zaeh, *Results Mater.* **2022**, *15*, 100305.

[34] A. Fröhlich, D. Gresens, B. Vervoort, K. Dröder, *Procedia CIRP* **2020**, *93*, 143.

[35] F. Konwitschny, J. Schnell, G. Reinhart, *Procedia CIRP* **2019**, *81*, 1236.